



HAL
open science

Direct comparison between a non orographic gravity wave drag scheme and constant level balloons

Francois Lott, Raj Rani, Aurélien Podglajen, Francis Codron, Lionel Guez, Albert Hertzog, Riwal Plougonven

► **To cite this version:**

Francois Lott, Raj Rani, Aurélien Podglajen, Francis Codron, Lionel Guez, et al.. Direct comparison between a non orographic gravity wave drag scheme and constant level balloons. *Journal of Geophysical Research: Atmospheres*, 2023, 128 (4), pp.e2022JD037585. 10.1029/2022JD037585 . hal-03857116v2

HAL Id: hal-03857116

<https://hal.science/hal-03857116v2>

Submitted on 15 Dec 2022

HAL is a multi-disciplinary open access archive for the deposit and dissemination of scientific research documents, whether they are published or not. The documents may come from teaching and research institutions in France or abroad, or from public or private research centers.

L'archive ouverte pluridisciplinaire **HAL**, est destinée au dépôt et à la diffusion de documents scientifiques de niveau recherche, publiés ou non, émanant des établissements d'enseignement et de recherche français ou étrangers, des laboratoires publics ou privés.

Direct comparison between a non orographic gravity wave drag scheme and constant level balloons

F. Lott¹, R. Rani¹, A. Podglajen¹, F. Codron², L. Guez¹, A. Hertzog³, and R. Plougonven⁴.

¹Laboratoire de Météorologie Dynamique (LMD)/IPSL, PSL Research Institute, Ecole Normale Supérieure, Paris, France.

²LOCEAN/IPSL, Sorbonne Université/IRD/MNHN/CNRS, Paris, France.

³LMD/IPSL, Sorbonne Université, Paris, France.

⁴LMD/IPSL, Ecole Polytechnique, Institut Polytechnique de Paris, Palaiseau, France

Key Points:

- A non-orographic parameterization tuned to produce a realistic tropical quasi-biennial oscillation is used to predict in-situ observations
- Parameterized gravity waves needed in large-scale models have realistic amplitudes in the tropical lower stratosphere
- Day-to-day variations of the estimated gravity wave momentum fluxes correlate well with observations

Corresponding author: Francois Lott, flott@lmd.ens.fr

Abstract

17 The parameterization scheme that represents gravity waves due to convection in LMDz-
18 6A, the atmospheric components of the IPSL coupled climate model (IPSLCM6), is di-
19 rectly compared to Strateole-2 balloon observations made in the lower tropical strato-
20 sphere from November 2019 to February 2020. The input meteorological fields necessary
21 to run the parameterization offline are extracted from the ERA5 reanalysis and corre-
22 spond to the instantaneous meteorological conditions found underneath the balloons. In
23 general, we find a fair agreement between measurements of the momentum fluxes due
24 to waves with periods less than 1 hr and the parameterization. The correlation of the
25 daily values between the observations and the results of the parameterization is around
26 0.4, which is statistically elevated considering that we analyse around 600 days of data
27 and surprisingly good considering that the parameterization has not been tuned: the scheme
28 is just the standard one that helps producing a Quasi-Biennial Oscillation in the IPSLCM6
29 model. Online simulations also show that the measured values of momentum fluxes are
30 well representative of the zonally and averaged values of momentum fluxes needed in LMDz-
31 6A to simulate a QBO. The observations also show that longer waves with periods smaller
32 than a day carry about twice as much flux as waves with periods smaller than an hour,
33 which is a challenge since the low period waves that make the difference are potentially
34 in the grey zone of most climate models.
35

Plain Language Summary

36
37 In most large-scale atmospheric models, gravity wave parameterizations are based
38 on well understood but simplified theories and parameters which are keyed to reduce sys-
39 tematic errors on the planetary scale winds. In the equatorial regions, the most challeng-
40 ing errors concern the quasi biennial oscillation. Although it has never been verified di-
41 rectly, it is expected that the parameterizations tuned this way should transport a re-
42 alistic amount of momentum flux in both the eastward and westward directions when
43 compared to direct observations. Here we show that it is the case, to a certain extent,
44 using constant-level balloon observations at 20 km altitude. The method consists in com-
45 paring directly, each day and at the location of the balloon the measured momentum fluxes
46 and the estimation of a gravity wave parameterization using observed values of the large-
47 scale meteorological conditions of wind, temperature and precipitation.

48 1 Introduction

49 It is well known that precipitation forces gravity waves (GWs) that propagate in
 50 the stratosphere (Fovell et al., 1992; Alexander et al., 2000; Lane & Moncrieff, 2008). These
 51 waves carry horizontal momentum vertically and interact with the large scale flow when
 52 they break. The horizontal scale of these waves can be quite short, much shorter than
 53 the horizontal scale of General Circulation Models (GCMs) so they need to be param-
 54 eterized (Alexander & Dunkerton, 1999). Although there are other sources of gravity waves
 55 that need to be parameterized, like mountain waves (Palmer et al., 1986; Lott, 1999) and
 56 frontal waves (Charron & Manzini, 2002; Richter et al., 2010; de la Cámara & Lott, 2015),
 57 the convective GWs are believed to dominate largely in the tropics. In these regions, they
 58 contribute significantly to the forcing of the Quasi-Biennial Oscillation (QBO), a near
 59 28-month oscillation of the zonal mean zonal winds that occurs in the lower part of the
 60 equatorial stratosphere (Baldwin et al., 2001). For these reasons, the parameterization
 61 of convective GWs is necessary for most GCMs to explicitly realize the QBO.

62 Although convective gravity wave parameterizations are now used in many mod-
 63 els with success (Beres et al., 2005; Song & Chun, 2005; Lott & Guez, 2013; Bushell et
 64 al., 2015), their validation using direct in situ observations remains a challenge. There
 65 exist observations of GWs using global satellite observations (Geller et al., 2013) but the
 66 GWs identified this way still have quite large horizontal scales, and some important quan-
 67 tities like the Momentum Fluxes (MFs) are often deduced indirectly, for instance from
 68 temperature measurements using polarization relations (Alexander et al., 2010; Ern et
 69 al., 2014). For these two reasons, in situ observations are essential, and the most pre-
 70 cise ones are provided by constant-level long-duration balloons, like those made in the
 71 Antarctic region during Strateole-Vorcore (Hertzog, 2007) and Concordiasi (Rabier et
 72 al., 2010), or in the deep tropics during PreConcordiasi (Jewtoukoff et al., 2013) and more
 73 recently Strateole 2 (Haase et al., 2018). Among many important results, these balloon
 74 observations have shown that the momentum flux entering in the stratosphere is extremely
 75 intermittent (Hertzog et al., 2012). This intermittency implies that the mean momen-
 76 tum flux is mostly transported by few large-amplitude waves that potentially break at
 77 lower altitudes than when the GW field is more uniform. This property, when reproduced
 78 by a parameterization (de la Cámara et al., 2014; Kang et al., 2017; Alexander et al.,
 79 2021), can help reduce systematic errors in the midlatitudes, for instance on the timing
 80 of the final warming in the Southern Hemisphere polar stratosphere (de la Cámara et
 81 al., 2016), or on the QBO (Lott et al., 2012). Balloon observations have also been used
 82 to characterize the dynamical filtering by the large scale winds (Plougonven et al., 2017),
 83 and to validate the average statistical properties of the GW momentum flux predicted
 84 offline using reanalysis data (Kang et al., 2017; Alexander et al., 2021).

85 However, to the best of our knowledge, the evaluation of parameterizations using
 86 balloon observations have remained quite indirect so far, with the common belief that
 87 the best a parameterization can do is to reproduce a realistic statistical behaviour (Jewtoukoff
 88 et al., 2015; Kang et al., 2017; Alexander et al., 2021). The fact that a parameterization
 89 could be used to simulate the observed momentum flux at a given time and place has
 90 never been tried, and there are few good reasons for that. For example, parameteriza-
 91 tions are often based on simplified quasi-linear wave theory, they assume spectral dis-
 92 tributions that are loosely constrained, and they ignore lateral propagation almost en-
 93 tirely (some attempt to include it can be found in Amemiya and Sato (2016)). Never-
 94 theless, some factors could mitigate these weaknesses. One is that in most parameter-
 95 izations the wave amplitude is systematically limited by a breaking criterion that encap-
 96 sulates nonlinear effects. An other is that many parameterizations explicitly relate launched
 97 waves to sources, and there is constant effort to improve the realism of the convective
 98 ones (Liu et al., 2022). Also, observations systematically suggest that dynamical filter-
 99 ing by the large scale wind is extremely strong for upward propagating GWs (Plougonven
 100 et al., 2017), and this central property is represented in most GW parameterizations. For

all these reasons, it may well be that a GW parameterization keyed to the large scale conditions found at a given place and time gives MFs that can be directly compared to the MFs measured by a balloon at the same place.

Based on the relative success of the offline calculations done in the past using re-analysis data (Jewtoukoff et al., 2015; Kang et al., 2017; Alexander et al., 2021), the purpose of this paper is to attempt such a direct comparison using the most recent observations. We will use for that the balloons of the first Strateole 2 campaign that flew in the lower tropical stratosphere between November 2019 and February 2020 (Corcos et al., 2021). For each of these flights and each time, we will identify the grid point in the ERA5 reanalysis (Hersbach et al., 2020) that is the nearest and used the vertical profiles of wind and temperature as well as the surface value of precipitation to emulate the Lott and Guez (2013)’s (LG13) parameterization of convective GWs. The plan of the paper is as follows. Section 2 describes the methodology used, section 3 analyzes in-depth the statistics and compares with online simulations. A summary with discussion on the method and some perspectives is provided in section 4.

2 Data and method

2.1 Parameterization of convective gravity waves

We take the LG13 parameterization of non-orographic gravity waves forced by convection that is operational in LMDz6-A (Hourdin et al., 2020) the atmospheric component of the IPSL Earth System model used to complete the CMIP6 experiments (IPSLCM6, Boucher et al. (2020)). This version of the parameterization is also used for the LMDz-6A experiments carried out in the frame of the QBO intercomparison project (QBOi) (Bushell et al., 2022; Holt et al., 2022). Among the salient aspects of the scheme, one is that it is multiwave and stochastic, the subgrid scale GW field (e.g., vertical wind disturbance w') being represented by stochastic Fourier series of monochromatic waves,

$$w'(x, y, t, z) = \sum_{n=1}^{\infty} C_n \hat{w}_n(z) e^{i(\mathbf{k}_n \cdot \mathbf{x} - \omega_n t)}, \quad (1)$$

where the intermittency parameters satisfy $\sum_{n=1}^{\infty} C_n^2 = 1$, and where \mathbf{k}_n and ω_n are the horizontal wave vector and frequency respectively. To determine the wave amplitude the variance of the subgrid scale precipitation field, P' , is assumed to compare in amplitude with the gridscale averaged precipitation P by writing

$$P' = \sum_{n=1}^{\infty} C_n P e^{i(\mathbf{k}_n \cdot \mathbf{x} - \omega_n t)}. \quad (2)$$

We then translate precipitation into diabatic heating which we distribute vertically over a fixed depth Δz in the troposphere. For each harmonic the heating produces a GW whose MF varies with the square of the precipitation P^2 times a tuning parameter G_{uw0} (see Equation 9, in LG13) and which is imposed at a fixed launching altitude z_l . Three factors then limit vertical propagation, (i) the presence of critical levels, (ii) a dissipative term controlled by a kinematic viscosity ν , and (iii) a criterion for saturation controlled by a saturation parameter S_c . All these effects are summarized in Equation 12 of LG13, but to illustrate how the background flow controls the outcome of the scheme, we recall the third criterion that saturation limits the amplitude of the momentum flux transported by each harmonic to values below

$$|\rho \hat{\mathbf{u}}_n \hat{w}_n^*| \leq \rho_r S_c^2 \frac{|\mathbf{k}_n \cdot (\mathbf{c}_n - \mathbf{U}(z))|^3}{N(z)} \frac{k_m}{|\mathbf{k}_n|^4}, \quad (3)$$

where the star stands for the complex conjugate, $\hat{\mathbf{u}}_n$ the harmonic of the horizontal wind vector disturbance, and $\mathbf{U}(z)$ and $N(z)$ the vertical profiles of horizontal wind vector and

142 buoyancy frequency respectively. Still in Equation 3 the reference density $\rho_r = 1\text{kgm}^{-3}$
 143 and k_m is the the minimal horizontal wavelength that needs to be parameterized: its in-
 144 verse scales the gridcell horizontal size. Compared to LG13, we have slightly rewritten
 145 the saturation criteria to make explicit that the saturated MF has small amplitude when
 146 the intrinsic phase speed amplitude in the wavevector direction $|\mathbf{k}_n \cdot (\mathbf{c}_n - \mathbf{U})|$ is small,
 147 the absolute horizontal phase speed being $\mathbf{c}_n = \mathbf{k}_n \omega_n / |\mathbf{k}_n|^2$. This mechanism is referred
 148 to as dynamical filtering in the following and is probably central in explaining the good
 149 correlations we describe next between the observed and parameterized MFs.

150 In practice, we make a distinction between the time scale of the life cycle of the waves
 151 Δt which we consider to be shorter than one day and the physical time step that sep-
 152 arates two calls of the parameterization, and which is around $\delta t = 10\text{mn}$ online. This
 153 distinction permits to launch few waves each time-step, typically $J = 8$, and to accu-
 154 mulate their effect over the day via an AR-1 process with decorrelation time of one day.
 155 On average and each day, the GW field is then made of $J \frac{\Delta t}{\delta t} \approx 1000$ harmonics, a num-
 156 ber we judge sufficient for a realistic representation. In the offline comparison we will
 157 not use such a large number of waves, essentially because it makes little sense to inter-
 158 polate ERA5 along 10mn intervals, but we will still launch 8 waves per hour to leave the
 159 scheme unchanged and average over the day. To test if the reduction in terms of num-
 160 ber of harmonics has significant impact we have rather made statistics averaging the pa-
 161 rameterization results over 9 adjacent gridpoints. In this case the number of harmon-
 162 ics involved becomes comparable to that used online and we did not find large qualita-
 163 tive differences. For completeness, we recall here the operational values of the different
 164 tuning parameters of the scheme used for CMIP6,

$$z_l = 5\text{km}, \Delta z = 1\text{km}, G_{uw0} = 0.23, S_c = 0.6, \rho_r = 1\text{kg/m}^3, k_m = 0.02\text{km}^{-1}. \quad (4)$$

165 The scheme selects randomly the horizontal wave number between $k_s < k < k_m$ us-
 166 ing uniform distribution and select the intrinsic phase speed at the launch level z_s ac-
 167 cording to a Gaussian distribution with standard deviation C_M . The operational val-
 168 ues for these parameters are,

$$k_s = 1\text{km}^{-1}, C_M = 30\text{m/s}, z_s = 5\text{km}. \quad (5)$$

169 It is important to emphasize that the scheme selects phase speeds rather than frequency,
 170 whereas the balloon data measure MFs as a function of intrinsic frequency. We there-
 171 fore analysed the characteristic distribution of the intrinsic frequency of the parameter-
 172 ized waves that enter in the stratosphere and verified that more than 75% of the param-
 173 eterized momentum fluxes are carried by harmonics with intrinsic period around and be-
 174 low 1hr (not shown). Note also that in its operational version, and to limit computational
 175 costs, only waves with horizontal wavenumber in the zonal direction are launched.

176 2.2 Offline parameterization runs

177 To activate the scheme in offline mode we will use ERA-5 hourly data of precip-
 178 itation and 3-hourly data of winds, surface pressure and temperature at $1^\circ \times 1^\circ$ hori-
 179 zontal grid to mimic a large scale climate model resolution. Winds and temperature are
 180 then linearly interpolated on 1hr time step to be synchronised with precipitation. In the
 181 vertical we use data at 67 model levels, taking one every two ERA5 levels, to speed up
 182 calculations but also to mimic the vertical resolution we have in the LMDz-6A GCM and
 183 which is slightly below 1km (in ERA5 and around 20km the vertical resolution is around
 184 500m when all the 137 levels are considered).

185 2.3 Strateole 2 balloon observations

186 The in situ observations we use are from the 8 constant level balloon flights which
 187 flew between 18.5 and 20km altitude for about 2-3 months during the Nov. 2019-February

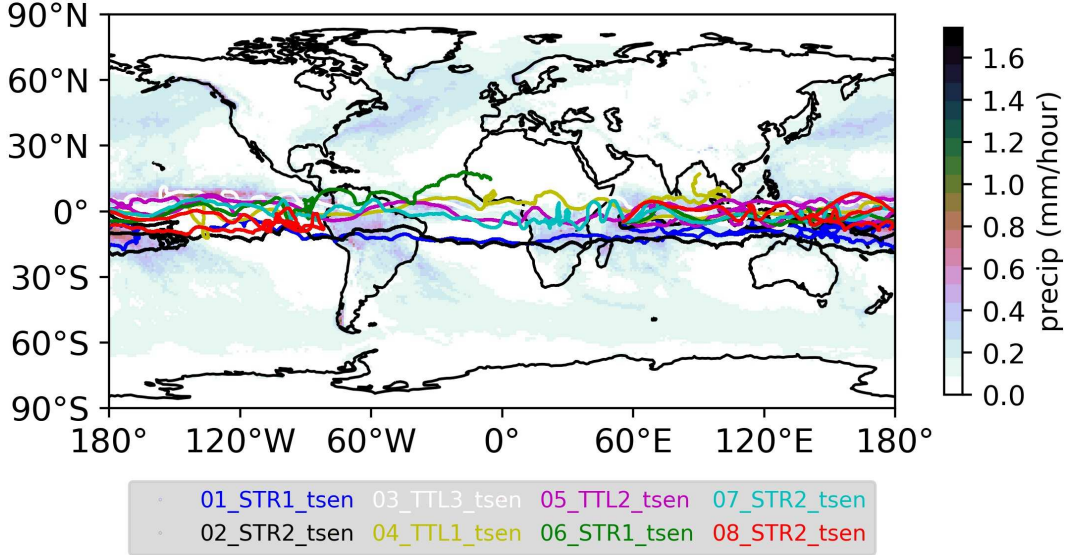


Figure 1. Strateole 2 balloon trajectories taking place between November 2019 and February 2020. Shading presents the precipitation field from ERA5 averaged over the period.

188 2020 periods of Strateole-2 (Corcos et al., 2021). Their trajectories are shown in Figure 1,
 189 superimposed upon the averaged precipitation. In the MFs calculated from observations
 190 Corcos et al. (2021) distinguish the waves with short periods (1hr-15mn) from the waves
 191 with period up to one day (1d-15mn). They also distinguish the eastward waves giving
 192 positive MF in the zonal direction from the westward waves giving negative MF, and from
 193 the MF amplitudes including all the directions of propagation. It is coincidental that the
 194 flights took place during the 2nd documented QBO disruption (Anstey et al., 2021), but
 195 the fact that the measurements are below the altitude at which the disruption manifests
 196 makes us believe that our comparison between gravity wave MFs over the period is not
 197 much affected by the disruption (beyond the fact that the disruption potentially affects
 198 the large scale winds, which is something that translates well in the parameterization).

199 In the following we will compare the momentum fluxes derived from the balloon
 200 data, emphasize the intrinsic frequencies that the scheme represents (the intrinsic peri-
 201 ods below 1hr) and consider the ERA5 data at the points that are the nearest from
 202 the balloon. The prediction is then made every hour and averaged over the day, again
 203 because this is the time scale needed for our scheme to sample realistically a GW field,
 204 and also because it takes around a day for a balloon flight to cover about a model grid-
 205 scale. We will discuss sensitivities to these choices in the first paragraph of the conclu-
 206 sion.

207 2.4 Online simulations

208 An important aspect of our work is that we use an operational scheme in offline
 209 mode without further tuning, a methodology that potentially impacts the amplitude of
 210 the MFs when compared to "free" model runs where dynamics and GWs evolve jointly.
 211 To measure the differences we will therefore compare offline and online calculations over
 212 around 3 QBO cycles (8 years). More precisely, we will make global estimations of the
 213 MFs and drag predicted offline using 8 years of ERA5 6hourly data (2013-2020). We will
 214 compare them to the MFs and drag issued from the LMDz-6A atmospheric model run-
 215 ning over the same period and at its medium resolution (144x143 regular longitude-latitude
 216 grid, 80 vertical levels with top at 1Pa). We first consider a "free run" , only forced with

217 the observed sea surface temperatures and sea-ice from the CMIP database, and the ozone
 218 climatology from the ACC/SPARC ozone database. This free run have the same settings
 219 of the parameterizations of orographic GWs (Lott, 1999), convective GWs (LG13), and
 220 GWs due to fronts and jet imbalances (de la Cámara & Lott, 2015) as those used for CMIP6
 221 (Hourdin et al., 2020). To make a smooth transition from the offline estimations with
 222 ERA5 to the free run done with LMDz-6A, we will also present a simulation with LMDZ-
 223 6A where the fields of horizontal wind and temperature are nudged toward ERA5 ev-
 224 ery 6hr with a relaxation constant of 1hr^{-1} .

225 3 Results

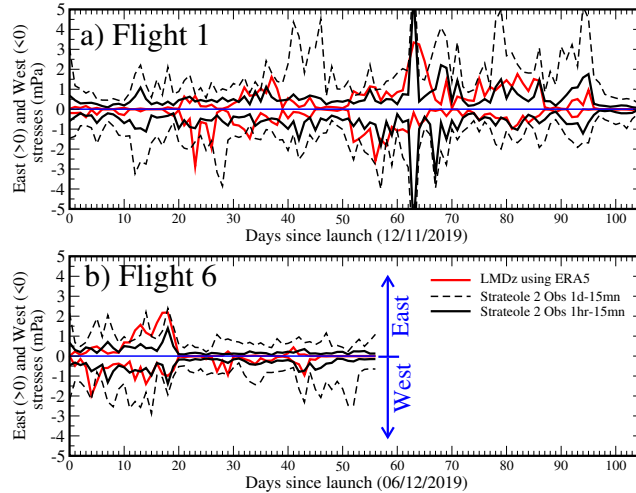


Figure 2. Comparison between daily averaged values of the eastward and westward MFs measured by the balloons and estimated by the GW scheme at the balloon location and altitude. Red curves are for the GW scheme predictions using ERA5, black curves are for the observed MFs due to the 15mn-1hr GWs, the thin dashed black curves are for MFs due to the 15mn-1day GWs.

226 3.1 Offline estimate of the observed values

227 Figure 2 shows time series of momentum fluxes measured during two balloon flights
 228 and the corresponding offline estimates. For clarity we present results for the Eastward
 229 and westward MF only, we will return more briefly to the accumulated MF and to the
 230 MF amplitude later. Note nevertheless that the operational GW scheme using only two
 231 directions of propagation, the accumulated MF is the sum of the eastward and westward
 232 MFs, the MF amplitude being their difference. Overall one sees in the two panels that
 233 the amplitudes of the momentum fluxes corresponding to the 1hr-15mn periods in the
 234 measurements compare well to the parameterized amplitudes in both the eastward and
 235 westward directions, the eastward and westward fluxes being of comparable amplitude
 236 but of opposite sign, as expected. For both, the observed momentum fluxes related to
 237 the 15mn-1day waves are substantially larger. In general and for flight 1 in Figure 2a,
 238 one sees that the parameterized fluxes are sometime small in amplitudes and in both di-
 239 rections (between the days 10 and 20), something that rarely happens in the observations.
 240 One also sees a tendency for the observed and estimated values to become larger jointly,
 241 like for instance the Eastward fluxes between days 60 and 95, before becoming small
 242 jointly afterward. This contrast between periods with larger and smaller MFs is even more
 243 pronounced in the flight 6 shown in Figure 2b. In it, one sees that the eastward and west-

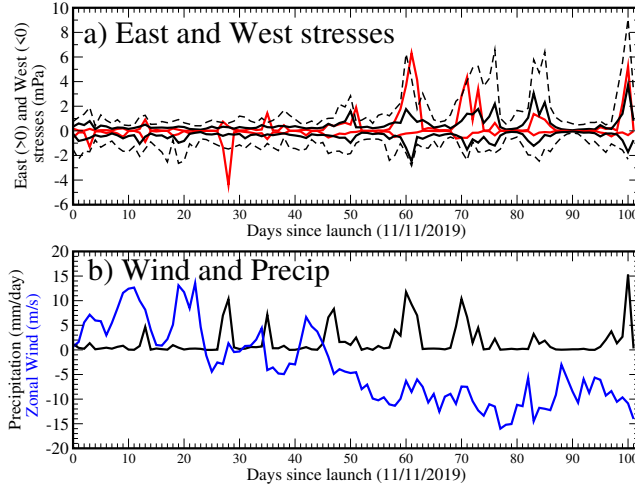


Figure 3. a) Same as Figure 2 but for Strateole Flight 2. b) ERA5 precipitations and zonal wind at the flight altitude.

244 ward MFs are quite large in amplitude before day 20, and are much smaller afterward.
 245 If we look at the trajectory in Figure 1 one sees that at its end, Flight 6 moves from the
 246 equatorial regions toward the subtropics and ends up over Sahel, i.e. a region of low pre-
 247 cipitation.

248 To give a better sense of what can cause the resemblances and differences between
 249 the observed MFs and their estimation, we plot in Figure 3a the eastward and westward
 250 MFs for flight 2, and in Figure 3b the precipitation and the (ERA5) zonal wind at the
 251 flight altitude. This is an interesting period since the zonal wind during this flight changes
 252 direction. Without a surprise, one sees in Figure 3 that the estimated flux peaks when
 253 the precipitation is large. One also sees that the MFs peaks are more pronounced in the
 254 direction opposed to the zonal wind consistent with the fact that waves with large am-
 255 plitude intrinsic phase speed can carry more momentum than waves with small intrin-
 256 sic phase speed (by dynamical filtering, see the first numerator in Equation 3). To a cer-
 257 tain extent, the relation with intense precipitation can be seen in the observations, mainly
 258 in the eastward direction after day 40. Dynamical filtering is also active for the measured
 259 fluxes, the observed westward fluxes being small compared to the eastward flux when
 260 the zonal wind becomes negative after day 50. Again, when the precipitation is small
 261 the simulated MFs are often small, whereas the observed ones always have non-zero back-
 262 grounds.

263 The fact that the parameterization estimates fluxes of about the right amplitude
 264 is summarized in Figure 4, where the average of the fluxes over the 8 entire flights are
 265 shown. It confirms systematically that the offline estimations are quite good on average
 266 and in the zonal direction, for the eastward and westward components again, but also
 267 on the accumulated flux (i.e the sum of the two and where the contributions from east-
 268 ward and westward propagating GWs largely oppose each other). In terms of stress am-
 269 plitudes one sees that the observations give larger value on average, but this is due to
 270 the fact that in Corcos et al. (2021) the amplitudes take into account the meridional com-
 271 ponents of the stress which are not included in the parameterization tested here. In the
 272 panel are also shown the correlations between the balloon averaged values of the stresses,
 273 they are often quite significant, despite the fact that only 8 flights are used.

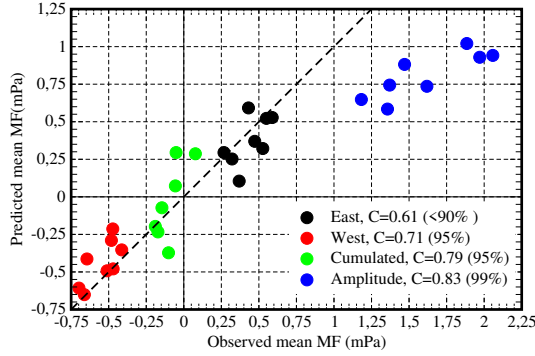


Figure 4. Scatter plot of the momentum fluxes measured by the balloon versus parametrized. Eight values are averages for the eight balloon flights. Significant test are for the correlation between the values, significance is estimated via a Pearson test with 6 degrees of freedom.

274 The curves in Figure 2 and Figure 3 also suggest that observations and offline es-
 275 timations evolve quite similarly day after day, both measured and parameterized MFs
 276 being sensitive to precipitation and dynamical filtering. To test more systematically this
 277 relationship, we next calculate the correlations between measured and estimated MFs
 278 and for each flight (Table 3.1). To test the significance, we measure the number of De-
 279 grees of Freedom (DoF) present in each dataset, and calculate for that the decorrelation
 280 time scale, which we take as the lag in day beyond which the lag-autocorrelation of the
 281 series falls below 0.2. As this time-lag varies from one series to the other, we give explic-
 282 itly in column 5, the number of DoF, which is the duration of the flight divided by the
 283 decorrelation time scale. Note that for their decorrelation time, we consider for simplic-
 284 ity that evaluated with daily averaged observations, but found that it is not much dif-
 285 ferent from that evaluated with the offline estimates (not shown). In each case, we find
 286 positive correlations, they are often significant in the Eastward direction and for the am-
 287 plitude, the estimated westward fluxes presenting more errors. Even weaker correlations
 288 occur for the accumulated stress, which most certainly reflects that in the accumulated
 289 stresses, large quantities of opposite sign balance one another, the resulting balance be-
 290 ing more difficult to predict.

291 As already mentioned, a defect of the scheme is it lacks background wave activity
 292 in the absence of precipitation. This means that momentum fluxes are underestimated
 293 in many circumstances, despite the fact that the amplitudes are realistic when consid-
 294 ering long term averages. To analyse better this difference and its potential consequences,
 295 the Figure 5 presents PDFs of the distributions of the momentum fluxes considering all
 296 the daily data. For the PDFs (solid line), one sees that the balloons almost systemat-
 297 ically measure fluxes with amplitude between 0.1mPa and 10mPa (see Figure 5a), whereas
 298 in the parameterization there are many more contributions from the smaller amplitude
 299 momentum fluxes (solid red), not mentioning that the zero values are excluded from PDFs
 300 when plotted versus the logarithm of MF amplitudes. To test if this difference in MF
 301 amplitude distribution has consequences, the dashed lines represent the contribution of
 302 a given MF value to the mean stress (which is just the PDF multiplied by the MF value
 303 itself). For the amplitudes, the values which actually contribute lie between 0.1mPa and
 304 10mPa in both the observations and the offline estimations. The fact that the small am-
 305 plitude waves are more frequent in the estimations is also true for the westward and east-
 306 ward components of the stress (Figures. 5b and 5c respectively). For both, nevertheless,
 307 the contribution to the average stress is due to larger amplitude waves in the estimations
 308 than in the observations, as indicated by the shifts towards larger values of the MFs be-
 309 tween the black dotted curve and the red dotted curve in Figures 5b and 5c.

Table 1. Correlation coefficient (24 hours averaged) between Strateole -2 Balloon flight (1hour15 min waves) and offline estimation (Notations for Significance Level: 99% : bold black with underline; 95%: bold black; 90% : solid; below 90%: solid italic). The significance are attributed following a Pearson test with degrees of freedom measured as the number of day divide by the decorrelation time of the series.

Flight	Altitude	Launch	End	Duration DOF	Cumulated	Amplitude	East	West
01_STR1	20.7	12/11/2019	28/02/2020	107/53	0.23	0.28	<u>0.46</u>	<i>0.07</i>
02_STR2	20.2	11/11/2019	23/02/2020	103/51	<i>0.21</i>	0.62	<u>0.62</u>	<i>0.05</i>
03_TTL3	19.0	18/11/2019	28/02/2020	101/33	0.49	0.42	<u>0.49</u>	0.43
04_TTL1	18.8	27/11/2019	02/02/2020	67/22	0.41	0.55	<u>0.55</u>	<u>0.53</u>
05_TTL2	18.9	05/12/2019	23/02/2020	79/19	0.36	<i>0.29</i>	0.36	<i>0.24</i>
06_STR1	20.5	06/12/2019	01/02/2020	57/10	<i>0.39</i>	0.67	<u>0.71</u>	0.59
07_STR2	20.2	06/12/2019	28/02/2020	83/16	<i>0.01</i>	<i>0.09</i>	<i>0.08</i>	<i>0.06</i>
08_STR2	20.2	07/12/2019	22/02/2020	77/12	<i>0.18</i>	0.7	<u>0.66</u>	<i>0.37</i>
ALL	x	x	x	670/170	0.30	0.41	<u>0.51</u>	<u>0.29</u>

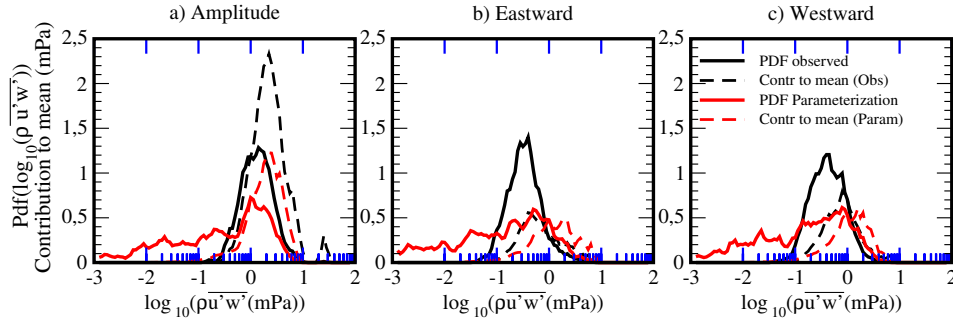


Figure 5. PDFs of daily values of momentum flux distribution (solid lines). The PDFs are calculated from histograms of 670 MFs daily value within intervals of $\Delta(\log_{10} \overline{\rho u'w'}) = 0.05$, thereafter smoothed by a 5 point non-recursive filter with weight (0.1, 0.2, 0.4, 0.2, 0.1). For the contribution of the waves to the MF (dashed lines), the PDF values are multiplied by the MF values $\overline{\rho u'w'}$ (in mPa). Measured values are in black, estimations using ERA5 data and the LG13 GWs parameterization are in red.

310

3.2 Global prediction and comparison with GCMs results

311

To appreciate whether the offline GW drag estimations using ERA5 are representative of the GWs MFs that a GCM requires to simulate a QBO, Figure 6a) presents time-altitude sections of the equatorial zonal winds and GWD predicted by the scheme globally and in offline mode between 2013-2020. In it we see that the gravity wave drag is negative (positive) where the zonal mean zonal wind vertical shear is negative (positive) consistent with the fact that it contributes to the descent of the QBO. We also note that the amplitudes vary between $\pm 0.5\text{m/s/day}$, a range characteristic of the parameterized GW tendency used in GCMs that produce a quasi-biennial oscillation (Butchart et al., 2018). The figure also indicates with a green rectangle the region and period during which the balloons operated.

 312
313
314
315
316
317
318
319
320

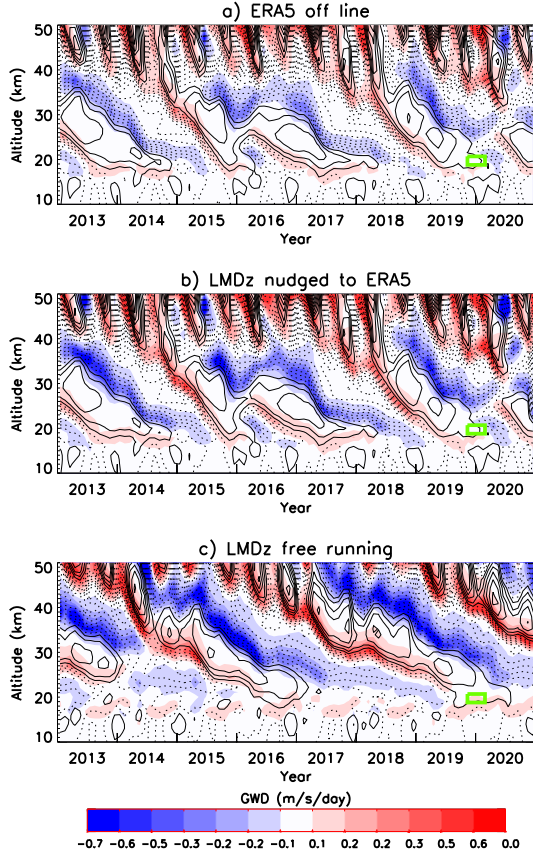


Figure 6. Time vertical sections of the zonal mean zonal wind ($CI=10m/s$, negative values dashed) and non orographic gravity wave drag zonal tendency (color) averaged over the equatorial band ($5^{\circ}S-5^{\circ}S$). Input data and GWD tendency are from a) ERA5 reanalysis and offline GWD scheme; b) LMDz-6A nudged to ERA5 and online GWD scheme; c) LMDz-6A free run an online GWD scheme. The green box indicates schematically the altitude and time ranges of the Strateole-2 flights considered in this study.

321 To check that comparable relations between GW drag and zonal wind shear occur
 322 in the LMDz-6A model, Figure 6b) first shows result from the nudged simulation. In it
 323 we see a strong resemblance in the GWD compared to the offline GWD in Figure 6a, the
 324 amplitudes being nevertheless substantially larger (around 25%) in the model. If we then
 325 look at the free run in Figure 6c) one sees again quite realistic relations between wind
 326 shears and drag, the GW drag is again substantially larger than that predicted using ERA5,
 327 despite the fact that the QBO period in LMDz-6A shown here is quite long (about 3 years
 328 here, LMDz-6A being a GCM with a long QBO (Bushell et al., 2022)). Note that this
 329 longer period could be reduced by enhancing the GW amplitude via for instance the tun-
 330 ing parameter G_{uw0} in Equation 4. Our experience with LMDz-6A is that the increase
 331 in G_{uw0} needed is of about few percents, a value that should not affect significantly the
 332 calculations done here with the operationnal scheme (not shown but for a systematic dis-
 333 cussion about tuning parameters and the QBO see Garfinkel et al. (2022)).

334 To address the differences in MFs globally, Figure 7a) shows the zonal mean of the
 335 eastward and westward MFs averaged over the equatorial band at 20km (i.e. about the
 336 balloon flights altitude) in the three runs, and the corresponding averaged precipitations
 337 (Figure 7b). The amplitude of the eastward and westward GW stresses are about 25%

338 and systematically larger in the free run (long dash) than in the offline test (solid), the
 339 nudged simulation being in between (dotted). Also interesting, the average of the stresses
 340 amplitude in the offline calculations are near $\pm 0.5\text{mPa}$, which is quite close to the av-
 341 erage value of the amplitude of the stresses estimated locally and measured during the
 342 balloon flights (see y values of the red and black dots in Figure 4).

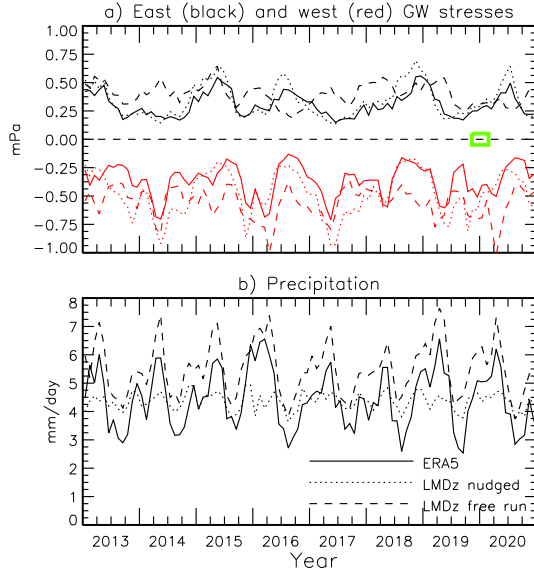


Figure 7. Time series of the $z = 20\text{km}$ zonal mean zonal non-orographic GW stresses and of the zonal mean precipitation averaged over the equatorial band (5°S - 5°S). Same input datas as in Figure 6.

343 As said in the introduction, the version of the parameterization used is operational
 344 in the atmospheric component of the IPSLCM6 model, and we have tried to change it
 345 as little as possible, which forces us to make choices. One is that we only call the param-
 346 eterization every hour in offline mode, using interpolated data from ERA5, rather than
 347 every 10mn in the model. Another is that LMDz-6A has a different grid yielding inter-
 348 polation errors that could make the behaviour of the parameterization very different be-
 349 tween ERA5 and LMDz-6A. Despite these differences it is remarkable that the errors are
 350 not outrageous, they also have a cause that is quite identifiable. In Figure 7b) one sees
 351 that in the free run, LMDz-6A overestimates by about 15% precipitation compared to
 352 ERA5, as in the scheme the sources use square precipitation (see Equation 9 in LG13),
 353 a 25% difference in the MFs is therefore not a surprise.

354 Interestingly also, the MFs in the nudged runs (dotted lines in Figure 7a) follow
 355 quite well the offline predictions. This is quite informative because in these nudged runs,
 356 the precipitation quite fails in representing an annual cycle (see the dotted line in Fig-
 357 ure 7b), which is probably due a mismatch between the nudged fields of temperature and
 358 winds and the model representation of diabatic processes. Although we did not analyse
 359 further the precipitation errors in these nudged runs, the fact that in them the MFs in
 360 Figure 4a) follows quite well the offline predictions is an indirect evidence that dynam-
 361 ical filtering plays a central role. Regarding that in Figures. 2-3 and in Table 3.1 the good
 362 correlations between predictions and balloon data seems in part related to the precipi-
 363 tation, it may be that globally such precise relationships are not necessarily needed, once
 364 about the right amount of precipitation is predicted.

365 4 Conclusion

366 The main result of this paper is that a state of the art parameterization of GWs
 367 due to convection reproduces reasonably well the momentum flux due to the high-frequency
 368 waves (periods between 15mn and 1hr) deduced from in situ measurements made onboard
 369 constant-level balloons. The parameterization represents well the eastward and westward
 370 values of the stress and their variations from day to day. We have made sensitivity tests,
 371 considering averages over 3hrs or 6hrs instead of a day, or/and averages over neighbour-
 372 ing points to increase the number of harmonics in the offline predictions and found lit-
 373 tle qualitative differences. For instance, averaging balloon data and predictions over shorter
 374 period, say 3hrs, result in much more noisy and decorrelated series, the correlation be-
 375 tween observations and measurements is lower but the DoF increase so the level of sig-
 376 nificance stays about the same as when using daily data as in Table 3.1. We have the
 377 impression that the best relations between observations and predictions are always for
 378 periods around a day and above. Note that this does not contradict our understanding
 379 of what a parameterization should do or a single balloon flight sample. In fact, a param-
 380 eterization like LG13 needs successive iterations to evaluate the large number of harmon-
 381 ics needed to represent realistically a GW field. Quite similarly, a balloon that progresses
 382 at a speed around 10m/s takes about 3 hours to travel through a 1° long model grid-
 383 cell, and this is just one transect. An ergodicity argument could be used to justify that
 384 averaging over a few 3-hours transects to cover a gridcell is equivalent to averaging the
 385 balloon data over 1day. This being said, we cannot exclude that better could be done
 386 with an other parameterization when considering shorter time scale. We nevertheless sus-
 387 pect that that the gain will not be to large in terms of correlation significance for instance,
 388 simply because the signals we handle are in essence extremely noisy. The daily averages
 389 we have done, on top of making some sense in the GW context help to increase the sig-
 390 nal/noise ratio.

391 Another important aspect of our work is that these results demonstrate that the
 392 GWs parameterization used in a large scale model to simulate a QBO parameterize MFs
 393 directly comparable with in situ observations. Although the measurements are extremely
 394 local, we verify that the average value they give is representative of the global values needed
 395 by a large-scale model to produce a QBOs. This is an important result in our opinion
 396 and for two reasons.

397 The first is that according to a common belief, there are discrepancies of a factor
 398 larger than 2 between the MFs parameterized in models and the global observations (Geller
 399 et al., 2013), at least in the mid-latitudes. In the equatorial regions, and using the same
 400 data as here, Corcos et al. (2021) gave bulk arguments to justify that the MF carried
 401 by the 15mn-1day waves is about what a model requires to generate a QBO. The change
 402 in region and the higher resolution of the observations could explain that the observa-
 403 tions now give larger but more realistic MFs, but we refine the results here and suggest
 404 that the contributions from the 15mn-1hr is sufficient. Of course this result should be
 405 refined, it may well be that LMDz-6A needs larger GW drag to decrease its QBO pe-
 406 riod or increase its intensity at lower altitudes. This is ongoing work, with a priority to
 407 include a background of GWs in LG13, and to optimize the scheme parameters using
 408 the available data. We also plan to test against balloon data the schemes used by the
 409 models that have contributed to QBOi. To be more complete quantitatively in terms of
 410 MFs, it is noticeable that we have not checked the contribution of the waves with pe-
 411 riod slower than 1day that should be explicitly resolved in the model, but we suspect it
 412 is quite small simply because the LMDz-6A spatial resolution is quite coarse (for an eval-
 413 uation of the large scale waves in LMDZ-6A see Maury and Lott (2014) and Holt et al.
 414 (2022)).

415 The second is that balloon measurements are extremely rare. Showing that they
 416 are representative of what occurs over much longer periods and over many different places
 417 suggests that they could be used, in conjunction with other products to provide much

418 larger datasets where GWs momentum fluxes and large scale conditions are combined.
 419 Among the datasets to consider, and on top of the satellite data (Ern et al., 2014; Alexan-
 420 der et al., 2021), the convection permitting global models look promising (Stephan et
 421 al., 2019), the gravity waves in the high resolution global models becoming more and more
 422 realistic (Sato et al., 1999; Shibuya & Sato, 2019). The huge datasets produced by these
 423 global models will become necessary if the tuning of GWs parameterization necessitate
 424 data assimilation techniques (Tandeo et al., 2015) and for the development of machine
 425 learning based parameterizations of GWs (Matsuoka et al., 2020; Chantry et al., 2021;
 426 Espinosa et al., 2022). For these, it seems crucial that physically based techniques can
 427 be validated against in situ data before shifting to machine learning techniques using syn-
 428 thetic data. We therefore plan to extend the analysis to the Loon LLC superpressure bal-
 429 loon data (Lindgren et al., 2020) which covers extratropical regions as well as tropical.
 430 It will permit to test, and maybe calibrate better, the orographic and frontal GWs pa-
 431 parameterizations used in LMDz-6A (Lott, 1999; de la Cámara & Lott, 2015).

432 5 Open Research

433 Balloon data presented in (Haase et al., 2018) can be extracted from the STRA-
 434 TEOLE 2 dedicated web site: <https://webstr2.ipsl.polytechnique.fr>

435 ERA5 reanalysis data are described in (Hersbach et al., 2020) and can be extracted
 436 from the COPERNICUS access hub: <https://scihub.copernicus.eu/>

437 The LMDz-6A GCM used for CMIP6 project is described in (Hourdin et al., 2020),
 438 it can be directly installed from the dedicated webpage: [https://lmdz.lmd.jussieu.fr/utilisateurs/installation-](https://lmdz.lmd.jussieu.fr/utilisateurs/installation-lmdz)
 439 [lmdz](https://lmdz.lmd.jussieu.fr/utilisateurs/installation-lmdz)

440 Acknowledgments

441 This work was supported by the VESRI Schmidt Future project DataWave.

442 References

- 443 Alexander, M. J., Beres, J. H., & Pfister, L. (2000). Tropical stratospheric grav-
 444 ity wave activity and relationships to clouds. *Journal of Geophysical Re-*
 445 *search: Atmospheres*, 105(D17), 22299-22309. doi: [https://doi.org/10.1029/](https://doi.org/10.1029/2000JD900326)
 446 [2000JD900326](https://doi.org/10.1029/2000JD900326)
- 447 Alexander, M. J., & Dunkerton, T. J. (1999). A Spectral Parameterization of Mean-
 448 Flow Forcing due to Breaking Gravity Waves. *J. Atmos. Sci.*, 56(24), 4167-
 449 4182. doi: 10.1175/1520-0469(1999)056<4167:ASPOMF>2.0.CO;2
- 450 Alexander, M. J., Geller, M., McLandress, C., Polavarapu, S., Preusse, P., Sassi,
 451 F., ... Watanabe, S. (2010). Recent developments in gravity-wave effects in
 452 climate models and the global distribution of gravity-wave momentum flux
 453 from observations and models. *Q. J. R. Meteorol. Soc.*, 136, 1103-1124. doi:
 454 <https://doi.org/10.1002/qj.637>
- 455 Alexander, M. J., Liu, C. C., Bacmeister, J., Bramberger, M., Hertzog, A., &
 456 Richter, J. H. (2021). Observational validation of parameterized gravity waves
 457 from tropical convection in the whole atmosphere community climate model.
 458 *Journal of Geophysical Research: Atmospheres*, 126(7), e2020JD033954.
 459 (e2020JD033954 2020JD033954) doi: <https://doi.org/10.1029/2020JD033954>
- 460 Amemiya, A., & Sato, K. (2016). A new gravity wave parameterization including
 461 three-dimensional propagation. *Journal of the Meteorological Society of Japan.*
 462 *Ser. II*, 94(3), 237-256. doi: 10.2151/jmsj.2016-013
- 463 Anstey, J. A., Banyard, T. P., Butchart, N., Coy, L., Newman, P. A., Osprey, S.,
 464 & Wright, C. J. (2021). Prospect of increased disruption to the QBO in a
 465 changing climate. *Geophysical Research Letters*, 48(15), e2021GL093058. doi:

- 466 <https://doi.org/10.1029/2021GL093058>
- 467 Baldwin, M. P., Gray, L. J., Dunkerton, T. J., Hamilton, K., Haynes, P. H., Randel,
468 W. J., . . . Takahashi, M. (2001). The quasi-biennial oscillation. *Rev. Geophys.*,
469 *39*(2), 179-229. doi: 10.1029/1999RG00007
- 470 Beres, J. H., Garcia, R. R., Boville, B. A., & Sassi, F. (2005). Implementa-
471 tion of a gravity wave source spectrum parameterization dependent on the
472 properties of convection in the whole atmosphere community climate model
473 (waccm). *Journal of Geophysical Research: Atmospheres*, *110*(D10). doi:
474 <https://doi.org/10.1029/2004JD005504>
- 475 Boucher, O., Servonnat, J., Albright, A. L., Aumont, O., Balkanski, Y., Bastrikov,
476 V., . . . Vuichard, N. (2020). Presentation and evaluation of the ipsl-cm6a-
477 lr climate model. *Journal of Advances in Modeling Earth Systems*, *12*(7),
478 e2019MS002010. doi: <https://doi.org/10.1029/2019MS002010>
- 479 Bushell, A. C., Anstey, J. A., Butchart, N., Kawatani, Y., Osprey, S. M., Richter,
480 J. H., . . . Yukimoto, S. (2022). Evaluation of the quasi-biennial oscilla-
481 tion in global climate models for the SPARC-QBO initiative. *Quarterly*
482 *Journal of the Royal Meteorological Society*, *148*(744), 1459-1489. doi:
483 <https://doi.org/10.1002/qj.3765>
- 484 Bushell, A. C., Butchart, N., Derbyshire, S. H., Jackson, D. R., Shutts, G. J.,
485 Vosper, S. B., & Webster, S. (2015). Parameterized gravity wave momen-
486 tum fluxes from sources related to convection and large-scale precipitation
487 processes in a global atmosphere model. *Journal of the Atmospheric Sciences*,
488 *72*(11), 4349-4371. doi: <https://doi.org/10.1175/JAS-D-15-0022.1>
- 489 Butchart, N., Anstey, J. A., Hamilton, K., Osprey, S., McLandress, C., Bushell,
490 A. C., . . . Yukimoto, S. (2018). Overview of experiment design and compar-
491 ison of models participating in phase 1 of the sparc quasi-biennial oscillation
492 initiative ("qboi"). *Geoscientific Model Development*, *11*(3), 1009-1032. doi:
493 10.5194/gmd-11-1009-2018
- 494 Chantry, M., Hatfield, S., Dueben, P., Polichtchouk, I., & Palmer, T. (2021). Ma-
495 chine learning emulation of gravity wave drag in numerical weather forecasting.
496 *Journal of Advances in Modeling Earth Systems*, *13*(7), e2021MS002477. doi:
497 <https://doi.org/10.1029/2021MS002477>
- 498 Charron, M., & Manzini, E. (2002). Gravity waves from fronts: Parameter-
499 ization and middle atmosphere response in a general circulation model.
500 *Journal of the Atmospheric Sciences*, *59*(5), 923 - 941. doi: 10.1175/
501 1520-0469(2002)059<0923:GWFFPA>2.0.CO;2
- 502 Corcos, M., Hertzog, A., Plougonven, R., & Podglajen, A. (2021). Observation of
503 gravity waves at the tropical tropopause using superpressure balloons. *Journal*
504 *of Geophysical Research: Atmospheres*, *126*(15), e2021JD035165. doi: <https://doi.org/10.1029/2021JD035165>
- 505
- 506 de la Cámara, A., & Lott, F. (2015). A parameterization of gravity waves emit-
507 ted by fronts and jets. *Geophys. Res. Lett.*, *42*(6), 2071-2078. doi: 10.1002/
508 2015GL063298
- 509 de la Cámara, A., Lott, F., & Hertzog, A. (2014). Intermittency in a stochastic
510 parameterization of nonorographic gravity waves. *J. Geophys. Res.: Atmo-*
511 *spheres*, *119*(21), 11905-11919. doi: 10.1002/2014JD022002
- 512 de la Cámara, A., Lott, F., Jewtoukoff, V., Plougonven, R., & Hertzog, A. (2016).
513 On the gravity wave forcing during the southern stratospheric final warming
514 in LMDZ. *J. Atmos. Sci.*, *73*(8), 3213-3226. doi: <https://doi.org/10.1175/JAS-D-15-0377.1>
- 515
- 516 Ern, M., Ploeger, F., Preusse, P., Gille, J., Gray, L. J., Kalisch, S., . . . Riese, M.
517 (2014). Interaction of gravity waves with the QBO: A satellite perspec-
518 tive. *Journal of Geophysical Research: Atmospheres*, *119*, 2329 - 2355. doi:
519 <https://doi.org/10.1002/2013JD020731>
- 520 Espinosa, Z. I., Sheshadri, A., Cain, G. R., Gerber, E. P., & DallaSanta, K. J.

- (2022). Machine learning gravity wave parameterization generalizes to capture the QBO and response to increased CO₂. *Geophysical Research Letters*, *49*(8), e2022GL098174. doi: <https://doi.org/10.1029/2022GL098174>
- Fovell, R., Durran, D., & Holton, J. R. (1992). Numerical simulations of convectively generated stratospheric gravity waves. *Journal of Atmospheric Sciences*, *49*(16), 1427 - 1442. doi: 10.1175/1520-0469(1992)049<1427:NSOCGS>2.0.CO;2
- Garfinkel, C. I., Gerber, E. P., Shamir, O., Rao, J., Jucker, M., White, I., & Paldor, N. (2022). A QBO cookbook: Sensitivity of the quasi-biennial oscillation to resolution, resolved waves, and parameterized gravity waves. *Journal of Advances in Modeling Earth Systems*, *14*(3), e2021MS002568. doi: <https://doi.org/10.1029/2021MS002568>
- Geller, M. A., Alexander, M. J., Love, P. T., Bacmeister, J., Ern, M., Hertzog, A., ... Zhou, T. (2013). A comparison between gravity wave momentum fluxes in observations and climate models. *J. Atmos. Sci.*, *26*(17).
- Haase, J. S., Alexander, M. J., Hertzog, A., Kalnajs, L. E., Deshler, T., Davis, S. M., ... Venel, S. (2018). Around the world in 84 days [Dataset]. *Eos*, *99*. doi: <https://doi.org/10.1029/2018EO091907>
- Hersbach, H., Bell, B., Berrisford, P., Hirahara, S., Hornyi, A., Muñoz-Sabater, J., ... Thpaut, J.-N. (2020). The ERA5 global reanalysis [Dataset]. *Quarterly Journal of the Royal Meteorological Society*, *146*(730), 1999-2049. doi: <https://doi.org/10.1002/qj.3803>
- Hertzog, A. (2007). The stratole-vorcore long-duration balloon experiment: A personal perspective. *Space Research Today*, *169*, 43-48. Retrieved from <https://www.sciencedirect.com/science/article/pii/S1752929807800478> doi: [https://doi.org/10.1016/S1752-9298\(07\)80047-8](https://doi.org/10.1016/S1752-9298(07)80047-8)
- Hertzog, A., Alexander, M. J., & Plougonven, R. (2012). On the Intermittency of Gravity Wave Momentum Flux in the Stratosphere. *Journal of the Atmospheric Sciences*(11), 3433-3448. doi: 10.1175/JAS-D-12-09.1
- Holt, L. A., Lott, F., Garcia, R. R., Kiladis, G. N., Cheng, Y.-M., Anstey, J. A., ... Yukimoto, S. (2022). An evaluation of tropical waves and wave forcing of the QBO in the QBOi models. *Quarterly Journal of the Royal Meteorological Society*, *148*(744), 1541-1567. doi: <https://doi.org/10.1002/qj.3827>
- Hourdin, F., Rio, C., Grandpeix, J.-Y., Madeleine, J.-B., Cheruy, F., Rochetin, N., ... Ghattas, J. (2020). LMDZ6A: The atmospheric component of the ipsl climate model with improved and better tuned physics [Software]. *Journal of Advances in Modeling Earth Systems*, *12*(7), e2019MS001892. doi: <https://doi.org/10.1029/2019MS001892>
- Jewtoukoff, V., Hertzog, A., Plougonven, R., de la Cámara, A., & Lott, F. (2015). Comparison of gravity waves in the southern hemisphere derived from balloon observations and the ecmwf analyses. *J. Atmos. Sci.*, *72*(9). doi: DOI:10.1175/JAS-D-14-0324.1
- Jewtoukoff, V., Plougonven, R., & Hertzog, A. (2013). Gravity waves generated by deep tropical convection: Estimates from balloon observations and mesoscale simulations. *Journal of Geophysical Research: Atmospheres*, *118*(17), 9690-9707. doi: <https://doi.org/10.1002/jgrd.50781>
- Kang, M.-J., Chun, H.-Y., & Kim, Y.-H. (2017). Momentum flux of convective gravity waves derived from an offline gravity wave parameterization. part i: Spatiotemporal variations at source level. *Journal of the Atmospheric Sciences*, *74*(10), 3167 - 3189. doi: 10.1175/JAS-D-17-0053.1
- Lane, T. P., & Moncrieff, M. W. (2008). Stratospheric gravity waves generated by multiscale tropical convection. *J. Atmos. Sci.*, *65*, 2598-2614. doi: DOI:10.1175/2007JAS2601.1
- Lindgren, E. A., Sheshadri, A., Podglajen, A., & Carver, R. W. (2020). Seasonal and latitudinal variability of the gravity wave spectrum in the lower

- 576 stratosphere. *Journal of Geophysical Research: Atmospheres*, 125(18),
 577 e2020JD032850. doi: <https://doi.org/10.1029/2020JD032850>
- 578 Liu, C., Alexander, J., Richter, J., & Bacmeister, J. (2022). Using trmm latent
 579 heat as a source to estimate convection induced gravity wave momentum
 580 flux in the lower stratosphere. *Journal of Geophysical Research: Atmo-*
 581 *spheres*, 127(1), e2021JD035785. (e2021JD035785 2021JD035785) doi:
 582 <https://doi.org/10.1029/2021JD035785>
- 583 Lott, F. (1999). Alleviation of stationary biases in a GCM through a moun-
 584 tain drag parameterization scheme and a simple representation of moun-
 585 tain lift forces. *Monthly Weather Review*, 127(5), 788 - 801. doi: 10.1175/
 586 1520-0493(1999)127<0788:AOSBIA>2.0.CO;2
- 587 Lott, F., & Guez, L. (2013). A stochastic parameterization of the gravity waves due
 588 to convection and its impact on the equatorial stratosphere. *J. Geophys. Res.*,
 589 118(16), 8897-8909. doi: 10.1002/jgrd.50705
- 590 Lott, F., Guez, L., & Maury, P. (2012). A stochastic parameterization of non-
 591 orographic gravity waves: Formalism and impact on the equatorial strato-
 592 sphere. *Geophys. Res. Lett.*, 39(6), L06807. doi: 10.1029/2012GL051001
- 593 Matsuoka, D., Watanabe, S., Sato, K., Kawazoe, S., Yu, W., & Easterbrook, S.
 594 (2020). Application of deep learning to estimate atmospheric gravity wave
 595 parameters in reanalysis data sets. *Geophysical Research Letters*, 47(19),
 596 e2020GL089436. doi: <https://doi.org/10.1029/2020GL089436>
- 597 Maury, P., & Lott, F. (2014). On the presence of equatorial waves in the lower
 598 stratosphere of a general circulation model. *Atmospheric Chemistry and*
 599 *Physics*, 14(4), 1869–1880. Retrieved from [https://acp.copernicus.org/](https://acp.copernicus.org/articles/14/1869/2014/)
 600 [articles/14/1869/2014/](https://acp.copernicus.org/articles/14/1869/2014/) doi: 10.5194/acp-14-1869-2014
- 601 Palmer, T. N., Shutts, G. J., & Swinbank, R. (1986). Alleviation of a system-
 602 atic westerly bias in general circulation and numerical weather prediction
 603 models through an orographic gravity wave drag parametrization. *Quar-*
 604 *terly Journal of the Royal Meteorological Society*, 112(474), 1001-1039. doi:
 605 10.1002/qj.49711247406
- 606 Plougonven, R., Jewtoukoff, V., de la Cámara, A., Lott, F., & Hertzog, A. (2017).
 607 On the relation between gravity waves and wind speed in the lower strato-
 608 sphere over the southern ocean. *J. Atmos. Sci.*, 74(4), 1075-1093. doi:
 609 10.1175/JAS-D-16-0096.1
- 610 Rabier, F., Bouchard, A., Brun, E., Doerenbecher, A., Guedj, S., Guidard, V.,
 611 ... Steinle, P. (2010, January). The Concordiasi Project in Antarctica.
 612 *Bulletin of the American Meteorological Society*, 91(1), 69-86. Retrieved
 613 from <https://hal-insu.archives-ouvertes.fr/insu-00562459> doi:
 614 10.1175/2009BAMS2764.1
- 615 Richter, J. H., Sassi, F., & Garcia, R. R. (2010). Toward a physically based gravity
 616 wave source parameterization in a general circulation model. *Journal of the At-*
 617 *mospheric Sciences*, 67(1), 136 - 156. doi: 10.1175/2009JAS3112.1
- 618 Sato, K., Kumakura, T., & Takahashi, M. (1999). Gravity waves appearing in a
 619 high-resolution GCM simulation. *Journal of the Atmospheric Sciences*, 56(8),
 620 1005 - 1018. doi: [https://doi.org/10.1175/1520-0469\(1999\)056\(1005:GWAI AH\)](https://doi.org/10.1175/1520-0469(1999)056(1005:GWAI AH)2.0.CO;2)
 621 2.0.CO;2
- 622 Shibuya, R., & Sato, K. (2019, 03). A study of the dynamical characteristics of
 623 inertiagravity waves in the antarctic mesosphere combining the pansy radar
 624 and a non-hydrostatic general circulation model. *Atmospheric Chemistry and*
 625 *Physics*, 19, 3395-3415. doi: 10.5194/acp-19-3395-2019
- 626 Song, I.-S., & Chun, H.-Y. (2005). Momentum flux spectrum of convectively
 627 forced internal gravity waves and its application to gravity wave drag pa-
 628 rameterization. part i: Theory. *J. Atmos. Sci.*, 62(1), 107-124. doi:
 629 <https://doi.org/10.1175/JAS-3363.1>
- 630 Stephan, C. C., Strube, C., Klocke, D., Ern, M., Hoffmann, L., Preusse, P., &

- 631 Schmidt, H. (2019). Intercomparison of gravity waves in global convection-
632 permitting models. *Journal of the Atmospheric Sciences*, 76(9), 2739 - 2759.
633 doi: 10.1175/JAS-D-19-0040.1
- 634 Tandeo, P., Pulido, M., & Lott, F. (2015). Offline parameter estimation using enkf
635 and maximum likelihood error covariance estimates: Application to a subgrid-
636 scale orography parametrization. *Quarterly Journal of the Royal Meteorological*
637 *Society*, 141(687), 383-395. doi: <https://doi.org/10.1002/qj.2357>